Dalton Transactions

ROYAL SOCIETY OF CHEMISTRY

PAPER

View Article Online
View Journal | View Issue

Check for updates

Cite this: *Dalton Trans.*, 2024, **53**, 6809

Mononuclear Fe(III) complexes with 2,4-dichloro-6-((quinoline-8-ylimino)methyl)phenolate: synthesis, structure, and magnetic behavior†

Ah Rim Jeong,[a] Si Ra Park,[b] Jong Won Shin,*[a] Jihyun Kim,[b] Ryuya Tokunaga,[c] Shinya Hayami [c] and Kil Sik Min *[b]

Received 30th December 2023,
Accepted 16th March 2024

DOI: 10.1039/d3dt04385a

rsc.li/dalton

Three Fe(III)-based coordination complexes $[Fe(dqmp)_2](NO_3)\cdot H_2O$ (**1**), $[Fe(dqmp)_2](BF_4)\cdot 2CH_3COCH_3$ (**2**), and $[Fe(dqmp)_2](ClO_4)$ (**3**) were synthesized from $Fe(NO_3)_3\cdot 9H_2O$/$Fe(ClO_4)_3\cdot xH_2O$, $NaBF_4$, and 2,4-dichloro-6-((quinoline-8-ylimino)methyl)phenol (Hdqmp) in methanol/acetone and characterized. The structures of complexes **1–3** were determined *via* single-crystal X-ray crystallography at 100 K and room temperature, and their magnetic properties in the solid and solution forms were investigated. All complexes showed meridional structures with two tridentate $dqmp^-$ ligands coordinated with Fe(III) cations. In the solid state, complex **1** showed an abrupt and complete spin crossover at 225 K, whereas complexes **2** and **3** exhibited an incomplete spin crossover at 135 and 150 K, respectively. In a dimethylformamide solution, the complexes showed counterion-dependent spin transitions. In contrast to the solid state, in solution, complex **1** did not exhibit complete spin crossover. However, complexes **2** and **3** showed more complete spin transitions in solutions than in the solid state. The relaxation times, T_1 and T_2, for **1** and **2** were determined and both increased with temperature from 220 to 380 K. The T_1 of **1** was larger than that of **2** at 380 K, and the T_1 values were larger than the T_2 values.

Introduction

Spin crossover (SCO) is a magnetic behavior generally exhibited by d^4–d^7 transition metal ions. It is a transition from high-spin to low-spin or *vice versa* induced by external stimuli such as temperature, light, and pressure. SCO has been extensively studied because of its potential applications in molecular sensors, molecular switches, displays, and contrast agents.[1] Fe(III) complexes with d^5 electron configurations are excellent candidates for SCO behavior because Fe(III) ions exhibit a large difference in the magnetic moment between high-spin (HS; $S = 5/2$) and low-spin (LS; $S = 1/2$) states and are rather stable in air.[2] In fact, the air stability of Fe(III) ions enables their use in diverse magnetic applications such as magnetic sensors and contrast agents.[3]

In this context, Fe(III) complexes based on *N*-(8-quinolinyl) salicylaldimine (Hqsal) have shown very prominent SCO behaviors and have been extensively investigated to reveal significant SCO phenomena.[4] The Hqsal ligand has a rigid and fixed geometry in a meridional fashion as a tridentate (Scheme 1). Interestingly, the ligand can form bis-type metal complexes and induce excellent SCO behavior in Fe(III) complexes. These complexes can be potentially stable and show SCO even in solutions. Harding *et al.* have reported a Fe(III) complex, $[Fe(qsal\text{-}I)_2]OTf$, with two qsal-I ligands (Hqsal-I = 5-iodo-*N*-(8-quinolyl)salicylaldimine), which first showed abrupt complete SCO at 228 K with 8 K hysteresis.[5] The cooperativity of hysteresis was attributed to the extensive π–π stacking and C–H···O/F hydrogen bonding. Mercuri *et al.* reported a Fe(III) dimeric complex $[Fe(qsal\text{-}5,7\text{-}Cl_2)(NCS)(MeO)]_2$ containing four qsal-5,7-Cl_2, two NCS^-, and two MeO^- species, which exists as a monomeric structure in solution.[6] This qsal-type complex showed a strong antiferromagnetic interaction through coordinated methoxide ions ($J = -21$ K). In contrast to monomeric qsal-type complexes, no SCO behavior was observed in this complex. Wang *et al.* reported four Fe(III) complexes, $[Fe(qsal\text{-}4\text{-}F)_2]Y$ (Y = NO_3^-, PF_6^-, BF_4^-, or OTf^-), with a new 4-fluoro-*N*-(8-quinolyl)salicylaldimine (Hqsal-4-F) ligand.[7] These complexes are monomeric species and exhibit SCO behaviors depending on the counter anions. For example, in

[a]*Department of Chemistry, Kyungpook National University, Daegu 41566, Republic of Korea. E-mail: jwshin@kisti.re.kr*
[b]*Department of Chemistry Education, Kyungpook National University, Daegu 41566, Republic of Korea. E-mail: minks@knu.ac.kr*
[c]*Department of Chemistry, Kumamoto University, Kumamoto 860-8555, Japan*

† Electronic supplementary information (ESI) available. CCDC 2002656–2002661. For ESI and crystallographic data in CIF or other electronic format see DOI: https://doi.org/10.1039/d3dt04385a

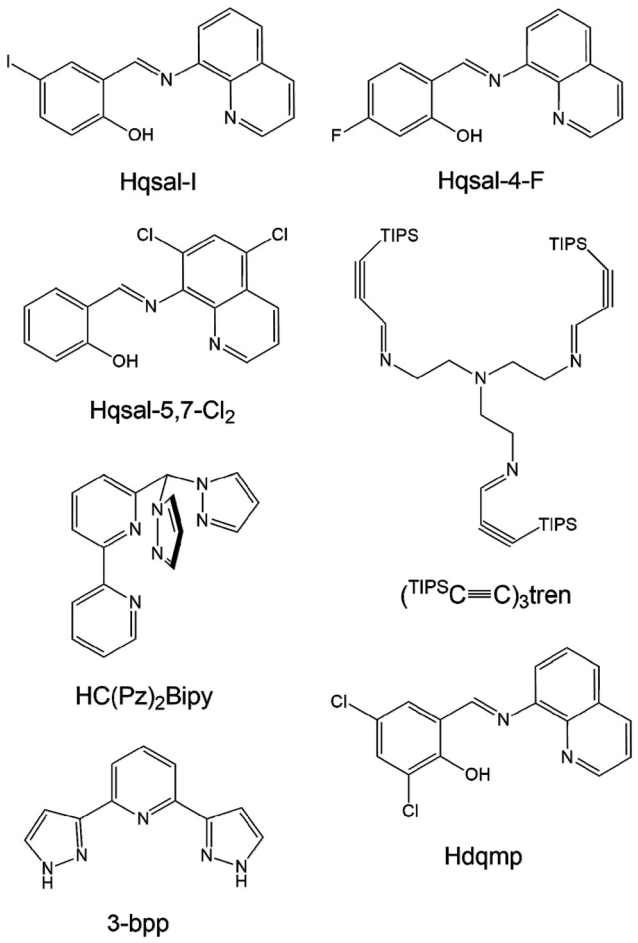

Scheme 1 Structures and abbreviations of multidentate ligands mentioned in the Introduction of this study.

the case of NO_3^-, two-step symmetry-breaking SCO was observed, whereas in the case of PF_6^-, a two-step gradual SCO was observed. Moreover, $[Fe(qsal\text{-}4\text{-}F)_2]BF_4$ underwent a gradual SCO, whereas $[Fe(qsal\text{-}4\text{-}F)_2]OTf$ almost entirely retained the HS state. These results indicate that the position of the substituent and the anions play critical roles in the SCO behavior of complexes.

Livesay and Shores reported a monomeric complex, $[((^{TIPS}C{\equiv}C)_3tren)Fe(OTf)_2]$ (Scheme 1), which is in the HS state at all temperatures in solids and solutions (*i.e.*, cyclopentanone, methanol, and dichloromethane).[8] However, it shows incomplete SCO with a $T_{1/2}$ value of 171 K in acetone, which is attributed to triflate dissociation upon decreasing temperature. Herres-Pawlis *et al.* reported bis(pyrazolyl)bipyridinylmethane Fe(II) complexes that exhibit various SCO behaviors in different solvents.[9] In acetonitrile or benzonitrile, the environment of the complex ion changed from N_5O to N_6, causing a temperature-dependent SCO behavior, which was different from the HS state of the solid sample. Barrett and Halcrow reported $[Fe(3\text{-}bpp)_2]X_2$ (3-bpp = 2,6-dipyrazol-3-ylpyridine), which exhibits versatile SCO behaviors at 259 K for X = BPh_4^- and 277 K for X = Br^- in acetone–water solvent.[10] The $T_{1/2}$ values of the salts of five anions exhibit a clear trend: $BPh_4^- \approx BF_4^- > CF_3SO_3^- > NO_3^- > Br^-$.

In the present study, the effects of the functional group of qsal ligands and anions on spin transition were investigated. We aimed to determine the changes in spin transition in solution through nuclear magnetic resonance (NMR) and confirm the possibility of the application of the prepared complexes as MRI contrast agents. Herein, we report three Fe(III) monomeric complexes, $[Fe(dqmp)_2](NO_3)\cdot H_2O$ (**1**), $[Fe(dqmp)_2](BF_4)\cdot 2CH_3COCH_3$ (**2**), and $[Fe(dqmp)_2](ClO_4)$ (**3**), which were prepared in methanol/acetone from Fe(III) salt and 2,4-dichloro-6-((quinoline-8-ylimino)methyl)phenol (Hdqmp) in air. These complexes exhibited octahedral monomeric structures and SCO in solid and solution states depending on the counteranion.

Experimental

General

All chemicals used in the synthesis were of reagent grade and used without further purification. Hdqmp was prepared as previously reported.[11] Infrared spectra were recorded using a Thermo Fisher Scientific Nicolet iS5 spectrophotometer (±1 cm^{-1}) with a KBr disk. Elemental analyses were performed using a Fisons/Carlo Erba EA1108 instrument in air. UV–vis absorption spectra were measured using a SCINCO S-2100 spectrophotometer. Magnetic susceptibilities were measured in an applied field of 5000 Oe between 5 and 300/400 K on a Quantum Design MPMS superconducting quantum interference device (SQUID) magnetometer. Diamagnetic corrections were made [417.78 (**1**), 407.20 (**2**), and 415.20 × 10^{-6} (**3**) emu mol^{-1}] using Pascal's constants.[12]

Syntheses of the compounds

$[Fe(dqmp)_2](NO_3)\cdot H_2O$ (1). Hdqmp (63 mg, 0.2 mmol) was dissolved in acetone (10 mL) in a test tube at room temperature. A methanol solution (3 mL) of $Fe(NO_3)_3\cdot 9H_2O$ (40 mg, 0.1 mmol) was added dropwise to the Hdqmp solution without agitation. After two days, the formed dark-brown crystals were filtered off, washed with methanol, and dried in air. Yield: 32 mg (42%). FT-IR (KBr, cm^{-1}): 3437, 3060, 2938, 1602, 1505, 1416, 1384, 1318, 1210, 1167, 768. Anal. calcd for $C_{32}H_{18}Cl_4FeN_5O_5$: C, 51.23; H, 2.42; N, 7.47. Found: C, 51.18; H, 2.16; N, 7.60.

$[Fe(dqmp)_2](BF_4)\cdot 2CH_3COCH_3$ (2). $NaBF_4$ (88 mg, 0.8 mmol) in MeOH (8 mL) was added under stirring to a solution of $Fe(NO_3)_3\cdot 9H_2O$ (162 mg, 0.4 mmol) in MeOH (4 mL) at room temperature. The mixture was slowly layered over a solution of Hdqmp (254 mg, 0.8 mmol) in acetone (20 mL). After several days, the formed dark-brown crystals of **2** were filtered off, washed with methanol, and dried in air. Yield: 250 mg (70%). FT-IR (KBr, cm^{-1}): 3437, 3067, 2929, 1606, 1508, 1419, 1319, 1056, 768. Anal. calcd for $C_{32}H_{18}BCl_4F_4FeN_4O_2$: C, 49.59; H, 2.34; N, 7.23. Found: C, 49.24; H, 2.51; N, 7.55.

[Fe(dqmp)$_2$](ClO$_4$) (3). Hdqmp (254 mg, 0.8 mmol) in acetone (10 mL) was added under stirring to a solution of Fe(ClO$_4$)$_3$·xH$_2$O (178 mg, 0.4 mmol, x = 5) in MeOH (10 mL) at room temperature. After several days, the formed dark-brown crystals of **3** were filtered off, washed with methanol, and dried in air. Yield: 170 mg (53%). FT-IR (KBr, cm^{-1}): 3436, 3067, 2928, 1603, 1506, 1418, 1319, 1211, 1169, 1089, 768, 622. Anal. calcd for $C_{32}H_{18}Cl_5FeN_4O_6$: C, 48.80; H, 2.30; N, 7.11. Found: C, 48.95; H, 2.38; N, 7.02.

X-ray crystallographic data collection and refinement

Single-crystal diffraction data of **1–3** were collected using their crystals at low and room temperatures, *i.e.*, 100(2) and 298(2) K for **1** and **2**, and 100(2) and 293(2) K for **3**. The crystal diffraction data obtained at the low temperature were designated as **1a**, **2a**, and **3a** and **1b**, **2b**, and **3b** at room temperature, respectively. The data were recorded using synchrotron radiation (λ = 0.70000 and 0.63000 Å) on an ADSC Quantum-210 detector at 2D SMC with a silicon (111) double-crystal monochromator at the Pohang Accelerator Laboratory, Korea. The ADSC Q210 ADX program[13] was used for data collection (detector distance: 62 mm, omega scan; $\Delta\omega$ = 1°, exposure time: 3 s per frame), and HKL3000sm (Ver. 703r)[14] was used for cell refinement, reduction, and absorption correction. The crystal structures of **1a**, **1b**, **2a**, **2b**, **3a**, and **3b** were solved by direct methods[15] and refined *via* full-matrix least-squares refinement using the SHELXL-2018 computer program.[16] The positions of all nonhydrogen atoms were refined using anisotropic displacement factors. All hydrogen atoms were placed using a riding model, and their positions were constrained relative to their parent atoms using the appropriate HFIX command in SHELXL-2018, except for the hydrogen atoms of water molecules. During the refinements of the structures (**2b**, **3a**, and **3b**), electron density peaks were located and believed to be highly disordered solvent molecules. All attempts to model the solvent molecules were unsuccessful, and they were removed using the SQUEEZE routine from PLATON software.[17] The SQUEEZE routine indicated that there were large solvent cavities and electrons: 495 Å^3 and 115 for **2b**, 700 Å^3 and 188 for **3a**, and 837 Å^3 and 198 for **3b**, per unit cell. In the final cycles of refinement, the contribution of electrons to the electron density was removed from the observed data. In **2b**, **3a**, and **3b**, the density, the F(000) value, the molecular weight and the formula were given without taking into account the results obtained with SQUEEZE. In addition, in the structure of **3**, the ClO$_4^-$ ion is disordered at 100 K. Thus, the oxygen atoms of **3a** were treated with 1.00 sof for one O atom and 0.75 sof for 4 O atoms. Unlike in **3a**, the perchlorate ion in **3b** at 293 K is well refined. The crystallographic data and the results of refinements of **1a**, **1b**, **2a**, **2b**, **3a**, and **3b** are summarized in Table S1.†

NMR measurements

A series of 1D ^{1}H NMR spectra were obtained using a Varian Unity INOVA NMR spectrometer (Korea Basic Science Institute, Western Seoul Center). All spectra were acquired using a 500 MHz NMR (11.7 T) spectrometer within a temperature range of 220–380 K. The Evans NMR spectra were recorded using custom-made NMR tubes with a pure solvent in the inner tube and the sample in the outer tube. For Evans NMR, the pure inner solvent residue was used as a reference. For the calculation of the magnetic data, the following equation was used: $\chi_g = (3\Delta f)/(4\pi m f)$, where Δf is the difference in chemical shift between residual proton signals [Hz], f is the spectrometer frequency [Hz], and m is the mass concentration of the paramagnetic sample [g cm^{-3}]. Additionally, χ_M was obtained by multiplying χ_g by the molar mass. Finally, we used the following equation to calculate the χ_M values: $\chi_M = (477\Delta\delta)/(2 \times 10^6 M)$, where χ_M is molar susceptibility [cm^3 mol^{-1}], $\Delta\delta$ is frequency shift [ppm], and M is molar concentration [mol L^{-1}].[1g,18] The NMR spectra for determining relaxation time were measured at the KAIST Analysis Center for Research Advancement using a 400 MHz (9.4 T) Agilent DD2 NMR spectrometer (Agilent Technologies Inc., Santa Clara, CA). The proton T_1 relaxation rates of dimethylformamide (DMF) in the presence of either **1** or **2** were determined using the inversion recovery method with 12 delays. For T_2 measurements, the Carr–Purcell–Meiboom–Gill (CPMG) pulse sequence was utilized, acquiring a total of 10–12 data points. Measurements were conducted at four temperatures: 220, 300, 340, and 380 K. Throughout the process, a recycle delay of 1 s was used. Raw data were processed and subjected to Fourier transformation using VnmrJ software (Agilent Technologies). Subsequently, peak integration and T_1 and T_2 curve fittings were performed using both VnmrJ software and Matlab (MathWorks, Natick, MA).

Results and discussion

Synthesis and characterization

Dark-brown complexes [Fe(dqmp)$_2$](NO$_3$)·H$_2$O (**1**) and [Fe(dqmp)$_2$](ClO$_4$) (**3**) were synthesized in yields of 42% and 53%, respectively, from a solution of Fe(NO$_3$)$_3$·9H$_2$O/Fe(ClO$_4$)$_3$·5H$_2$O and Hdqmp at room temperature in MeOH/acetone. At the same time, dark-brown [Fe(dqmp)$_2$](BF$_4$)·2CH$_3$COCH$_3$ (**2**) was prepared in high yield (70%) from Fe(NO$_3$)$_3$·9H$_2$O, NaBF$_4$, and Hdqmp at room temperature in MeOH/acetone. The prepared complexes were coordinated with two dqmp$^-$ ligands, causing distorted octahedral cationic species. However, the counterions of complexes **1**, **2**, and **3** were different: NO$_3^-$, BF$_4^-$, and ClO$_4^-$, respectively. The compositions of **1–3** were determined *via* elemental analyses, infrared spectroscopy, and single-crystal X-ray diffraction. The IR spectra of the complexes showed a common strong ν(CN) band at *ca.* 1604 ± 2 cm^{-1} which was assigned to the imine group of the dqmp$^-$ ligand. This band was consistent with coordination to the Fe^{III} center, as it shifted by *ca.* 17 cm^{-1} to lower energy compared with the free ligand Hdqmp. Stretches for the anions, NO$_3^-$, BF$_4^-$, and ClO$_4^-$, were also observed in the IR spectra, that is, strong bands of the counterions were noted at 1384 (NO$_3^-$), 1056 (BF$_4^-$), and 1089 cm^{-1} (ClO$_4^-$).[19]

Description of the crystal structures

The crystal structures of monomeric complexes [**1a**, **1b**, **2a**, **2b**, **3a**, and **3b**] were determined by X-ray crystallography at low

Table 1 Selected bond lengths (Å) and angles (°) for **1**, **2**, and **3**

	1a	1b	2a	2b	3a	3b
Fe1–N1	1.994(3)	2.194(3)	1.978(2)	2.014(3)	1.972(2)	1.986(3)
Fe1–N2	1.919(3)	2.093(3)	1.933(3)	1.942(4)	1.935(2)	1.938(3)
Fe1–N3	1.976(3)	2.124(3)	1.984(2)	2.019(4)	1.981(2)	1.974(3)
Fe1–N4	1.939(3)	2.138(3)	1.939(3)	1.950(4)	1.933(2)	1.940(3)
Fe1–O1	1.874(2)	1.923(2)	1.879(2)	1.882(3)	1.870(2)	1.880(2)
Fe1–O2	1.881(2)	1.910(3)	1.867(2)	1.873(3)	1.876(2)	1.870(2)

temperature (100 K, a) and at room temperature (298/293 K, b); the crystallographic data are summarized in Table S1,† and selected bond lengths are provided in Table 1. All complexes include isostructural monomeric $[Fe^{III}(dqmp)_2]^+$ cation with two tridentate dqmp$^-$ ligands that coordinated meridionally to each other, that is, two phenolate (and quinolones) groups were *cis* relative to each other and two imine nitrogen atoms were in a *trans* configuration. Complexes **1–3** contained NO_3^-, BF_4^-, and ClO_4^- anions, respectively. In addition, complexes **1** and **3** crystallized with water molecules as a lattice solvent, whereas complex **2** crystallized with acetone molecules. ORTEP drawings of **1a**, **2a**, and **3a** are shown in Fig. 1.

At 298 K, the average Fe–N and Fe–O bond lengths of **1** were 2.137(2) and 1.919(2) Å, respectively, which are typical of $[Fe(qsal\text{-}X)_2]^+$ in the HS state.[7,20] At 100 K, the average Fe–N and Fe–O bond lengths were 1.957(2) and 1.878(1) Å, respectively, which are consistent with those of a LS Fe^{III} center.[21] The changes in the average bond lengths between the structures at 298 and 100 K were ΔFe–N = 0.180 Å and ΔFe–O = 0.041 Å. These values are comparable with those reported for $[Fe(qsal)_2]I_3$ and $[Fe(qsal\text{-}OMe)_2]Cl_2{\cdot}MeOH{\cdot}0.5H_2O$ and indicate a complete SCO.[22] Different from the structure of **1**, the average Fe–N and Fe–O bond lengths of **2** were slightly changed depending on the temperature, that is, the changes in the average bond lengths between the structures at 298 and 100 K were ΔFe–N = 0.016 Å and ΔFe–O = 0.005 Å, which is indicative of an incomplete SCO. Based on the average Fe–N and Fe–O bond lengths, the spin state of **2** was very close to those of an LS Fe^{III} center in the $[Fe(qsal\text{-}X)_2]^+$ species.[7,20,21] Likewise, the average Fe–N and Fe–O bond lengths of **3** were very slightly changed due to temperature, that is, the changes in the average bond lengths between the structures at 298 and 100 K were ΔFe–N = 0.006 Å and ΔFe–O = 0.002 Å, and indicated an incomplete SCO. In this case, the spin state of **3** was nearly consistent with those of the LS Fe^{III} centers.[20,21]

At 100 K, the average bite distances and angles of the five-membered chelate rings were 2.587(3) Å and 82.73(8)° for **1**, 2.595(3) Å and 82.97(9)° for **2**, and 2.583(2) Å and 82.69(7)° for **3**, respectively. These are almost identical within the estimated standard deviations. This means the structures of **1–3** at 100 K were quite similar. At room temperature, the average bite distances and angles of the five-membered chelate rings were 2.646(3) Å and 76.47(8)° for **1**, 2.594(2) Å and 81.80(7)° for **2**, and 2.585(2) Å and 82.56(7)° for **3**, respectively. The distance and angle of **1** were quite different from those of **2** and **3**. This can be attributed to the high spin state of **1** at room temperature and the low spin states of **2** and **3** at room temperature. Additionally, we calculated the octahedral distortion parameters Σ and Φ of **1a–3b**.[23] The Σ and Φ values were 43.1 and 123.7° for **1a**, and 76.1 and 275.8° for **1b**, respectively. From the big difference of the Σ and Φ values between **1a** and **1b**, we have observed the structural change due to the spin transition. However, complexes **2** and **3** did not exhibit any significant changes for the Σ and Φ values (42.0 and 124.3° for **2a**, 41.3 and 129.0° for **2b**, 41.2 and 121.0° for **3a**, and 41.7 and 123.8° for **3b**, respectively).[23] These values are attributed to the very small transformation of the spin states.

All aromatic groups (*i.e.*, quinoline and benzene) of **1a** and **2a** were involved in π–π interactions with the adjacent aromatic groups of the neighboring Fe(III) complex. Owing to these π–π interactions, all Fe(III) complex ions were linked in a two-dimensional network extending along the $a(b + c)$ plane (Fig. 2 and 3). A ladder-like 1D chain structure was formed along axis *a*, due to the π–π interactions between the quinoline and benzene groups. In **1a**, the shortest centroid···centroid distance between two quinolines was 3.73 Å, and that between quinoline and benzene was 3.94 Å. Furthermore, the π–π interactions between the ladder-like 1D chains existed through two quinoline groups (centroid···centroid distance 3.47 Å), forming a 2D sheet structure (Fig. 2). In **2a**, the shortest centroid···centroid distance between two quinolines was 3.70 Å, and that between quinoline and benzene was 3.77 Å. Furthermore, the π–π interactions between the ladder-like 1D chains existed through two quinoline groups (centroid···centroid distance, 3.62 Å), inducing a 2D sheet structure (Fig. 3). In contrast to **1a**, within the ladder-like 1D chain of **1b**, the shortest centroid···centroid distance between two quinolines was 3.67 Å, and that between quinoline and benzene was 4.38 Å. Between the ladder-like 1D chains, the centroid···centroid distance was 3.59 Å through two quinoline groups. Contrary to **2a**, within a ladder-like 1D chain of **2b**, the shortest centroid···centroid distance between the two quinolines was 3.77 Å and that between quinoline and benzene was 3.87 Å. Between the ladder-like 1D chains, the centroid···centroid distance through two quinoline groups was 3.71 Å.

In the case of **3a**, owing to these π–π interactions, all Fe(III) complex ions were linked together, forming a two-dimensional network extending along the *bc* plane (Fig. 4). A 1D chain structure was formed along the *c* axis because of the π–π interactions between the quinoline groups. The shortest centroid···centroid distances of **3a** between the two quinolines were 3.52 and 3.66 Å, respectively. Furthermore, the π–π interactions between the 1D chains existed through the quinoline and benzene groups (centroid···centroid distance, 4.29 Å), inducing a 2D sheet structure. In contrast to **3a**, in a 1D chain of **3b**, the shortest centroid···centroid distances between the two quinolines were 3.66 and 3.57 Å, respectively. Between the 1D chains, the centroid···centroid distance was 4.33 Å through the quinoline and benzene groups. As mentioned above, the shortest centroid···centroid distances between two quinolines or between quinoline and benzene decreased in the ladder-like 1D chains in the order of complexes **1** > **2** > **3**. This means that

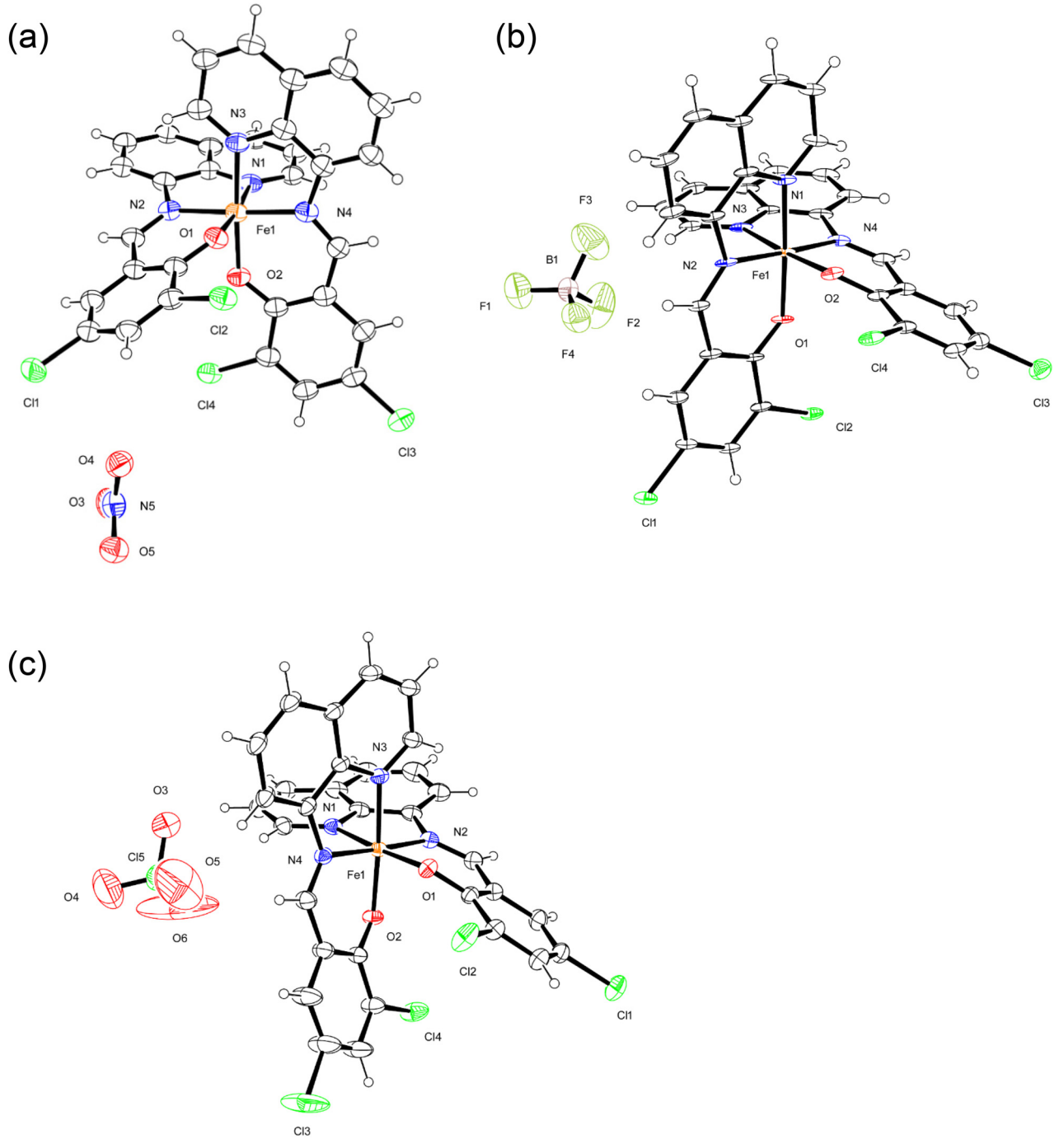

Fig. 1 ORTEP views of **1a** (a), **2a** (b), and **3a** (c). The atoms are represented by 40% (**1a** and **2a**) and 30% (**3a**) probable thermal ellipsoids. Solvent molecules were omitted for clarity.

they were densely stacked in the order of **1**, **2**, and **3**, and can be supported by suggesting that spin transition is difficult to occur in the order.

Magnetic properties of solids 1–3

Magnetic susceptibility, χ, of polycrystalline samples **1–3** at 2–300 K was measured at 5000 Oe on a SQUID magnetometer. At 300 K, the $\chi_M T$ value of **1** was *ca.* 4.09 emu K mol^{-1} and was almost constant until 224 K, which is the expected value for the HS Fe(III) ions (S = 5/2). Subsequently, $\chi_M T$ abruptly decreased to 0.463 emu K mol^{-1} at 204 K, indicating an SCO behavior (Fig. 5).[24] With further cooling, the $\chi_M T$ value very slightly decreased to 0.428 emu K mol^{-1} at 5 K, which is the expected value for the LS Fe(III) ion (S = 1/2).[25] With an increase in temperature from 5 to 300 K in the second run, $\chi_M T$ showed a similar trend to that in the first run, with a

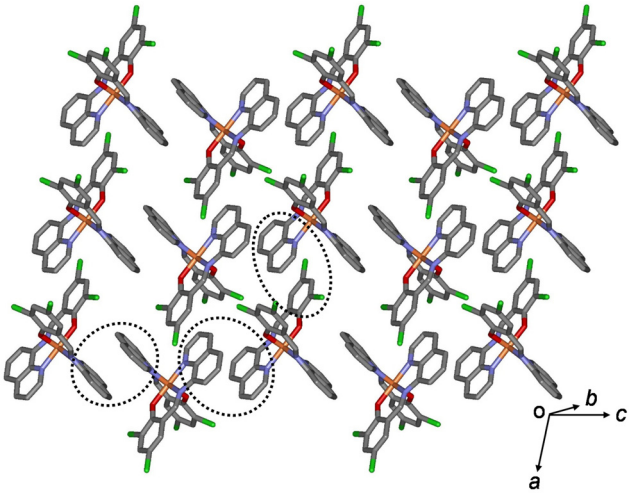

Fig. 2 Schematic of **1a**, showing an extended 2D layered structure formed *via* $\pi-\pi$ interactions (dotted circles).

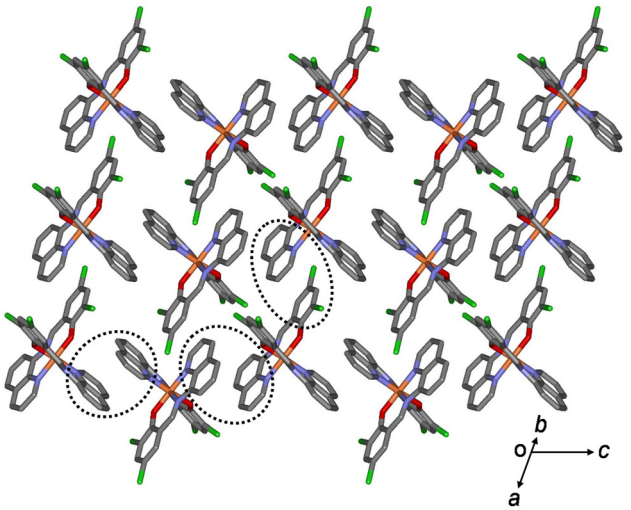

Fig. 3 Schematic of **2a**, showing an extended 2D layered structure formed *via* $\pi-\pi$ interactions (dotted circles).

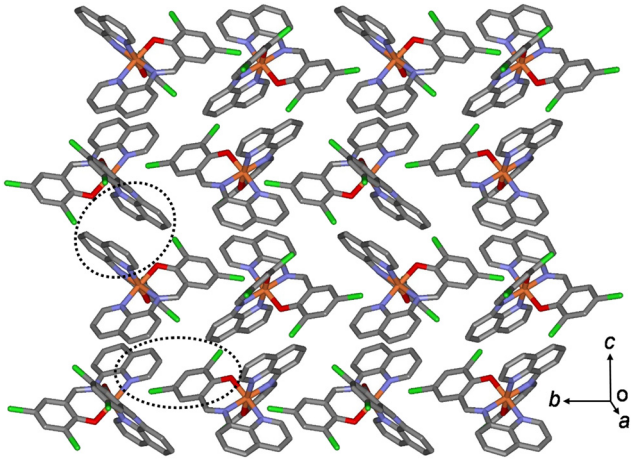

Fig. 4 Schematic of **3b**, showing an extended 2D layered structure formed *via* $\pi-\pi$ interactions (dotted circles).

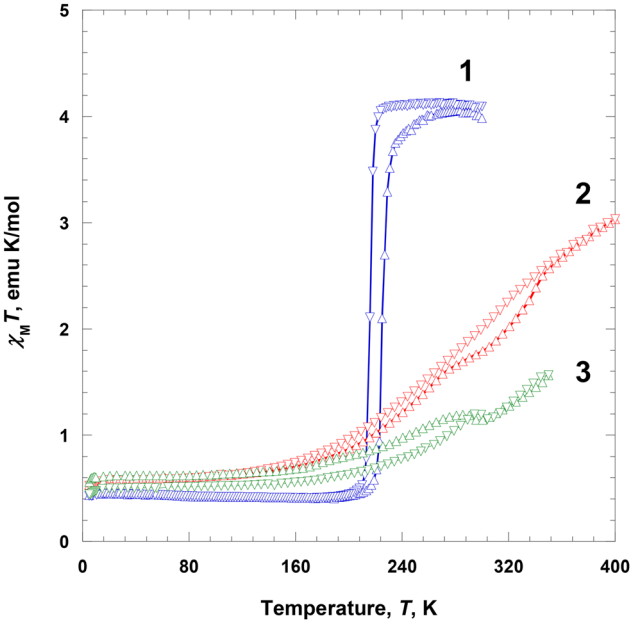

Fig. 5 Magnetic susceptibility data, displayed as the $\chi_M T$ product for **1–3** at 5000 Oe during heating (Δ) and cooling (∇).

small hysteresis. From 5 to 213 K, the $\chi_M T$ value gradually increased from 0.436 to 0.481 emu K mol^{-1}, followed by an abrupt increase to 3.85 emu K mol^{-1} at 241 K, indicating an SCO, and then further increased to 4.04 emu K mol^{-1} at 290 K. Thus, the critical temperatures during heating showed a thermal hysteresis with a width of approximately 9 K at 225 K. Interestingly, this complex shows spin transition that can be clearly stabilized in both HS and LS states.[1i,2c]

The $\chi_M T$ value of **2** at 5 K was 0.531 emu K mol^{-1} and was nearly constant until 135 K (0.658 emu K mol^{-1}), which is the expected value for the LS Fe(III) ions (S = 1/2). Subsequently, it rapidly increased to 3.03 emu K mol^{-1} at 400 K, indicating an SCO (Fig. 5).[24] The $\chi_M T$ value at 400 K was significantly lower than the expected spin-only value of 4.38 emu K mol^{-1}, indicating that the magnetic spin state at 400 K did not fully recover to the HS state of the Fe(III) ions (*ca.* 80% high spin).[20b] With a decrease in temperature from 400 to 5 K in the second run, $\chi_M T$ showed a similar trend to that in the first run, with a small hysteresis. With cooling from 400 to 135 K, the $\chi_M T$ value gradually decreased from 3.03 to 0.666 emu K mol^{-1}; with further cooling to 5 K, it decreased only slightly to 0.525 emu K mol^{-1}, which is the expected value for the LS Fe(III) ions (S = 1/2). In this case, the LS state at 5 K is fully recovered. In the region of SCO, there is a very small thermal hysteresis.

The $\chi_M T$ value of **3** at 5 K was 0.560 emu K mol^{-1} and was nearly constant until 150 K (0.670 emu K mol^{-1}), which is the expected value for the LS Fe(III) ions (S = 1/2), followed by a prominent increase to 1.19 emu K mol^{-1} at 285 K, indicating an

SCO (Fig. 5).[24] Between 285 and 300 K, a phase transition occurred with a very small decrease in $\chi_M T$. Above 300 K, the $\chi_M T$ value continuously increased with temperature until 350 K (1.56 emu K mol^{-1}). This indicates that the magnetic spin state at 350 K did not fully recover to the HS state of the Fe(III) ions (*ca.* 50% HS).[20b] With a decrease in temperature from 350 to 305 K in the second run, $\chi_M T$ showed a similar trend to that in the first run. Specifically, between 350 and 305 K, $\chi_M T$ gradually decreased from 1.57 to 1.15 emu K mol^{-1}, followed by a slight increase to 1.19 emu K mol^{-1} at 295 K. It then gradually decreased to 0.544 emu K mol^{-1} until 150 K, and remained almost constant until 5 K (0.544 emu K mol^{-1}), ultimately taking the expected value for the LS Fe(III) ions (S = 1/2).[24] The $\chi_M T$ curves obtained during heating and cooling exhibited a similar pattern; however, below 300 K, there was a small difference in magnetic moments, which was attributed to an annealing effect during heating.

In the crystalline solids of **1–3**, the completeness of spin transition in **1–3** decreased in the order of NO_3^- > BF_4^- > ClO_4^-, which was attributed to the size of the counter anions. With respect to the counter anions, the SCO behaviors can be related to the shape and size of each anion. Nitrate ion is planar and shows hydrogen bonds (C–H···O) that extend in three directions in **1**, whereas BF_4^-/ClO_4^- extends in four directions in **2** and **3**, respectively, and are tightly connected by hydrogen bonds (C–H···F/O). Thus, when it is spherical and has a large volume like BF_4^- or ClO_4^-, the Fe(III) species in the solid state can be disturbed to induce spin transition due to the increase of the volume of the Fe(III) ion. Finally, an SCO is more difficult to occur in **2** and **3** than in **1**.

Magnetic properties of the solutions of 1–3

Magnetic susceptibilities of the solution samples of **1–3** were measured in a DMF-d_7 solvent using an NMR spectrometer at several different temperatures during heating from 220 to 380 K (Fig. 6). The effective magnetic moment, $\mu_{eff}(T)$ [=$(8\chi_M T)^{1/2}$], was calculated using χ_M obtained using the Evans method (Tables S2–S4 and Fig. S1–S3†).[18] At 220 K, the $\mu_{eff}(T)$ value of **1** was *ca.* 2.38μ_B, which is slightly higher than that of the LS Fe(III) ion (S = 1/2). With the increase in temperature from 220 to 380 K, the effective moment gradually increased to 4.28μ_B. This indicates that the magnetic spin states at 380 K did not fully recover to the HS state of the Fe(III) ions (*ca.* 68% HS, assuming $\mu_{eff}(T)$ = 5.92μ_B).[26] This behavior is rather different from that in the solid state. Interestingly, **1** showed a complete SCO in the solid state, whereas the solution of **1** did not show a complete SCO, that is, the magnetic moment of **1** differed between the solid and solution forms. This means that the SCO behavior is related to crystal packing and solvent effects.[27]

At 220 K, the $\mu_{eff}(T)$ value of **2** was *ca.* 2.77μ_B, which is higher than that of the LS Fe(III) ions (S = 1/2) and close to the S = 1 spin state.[25] With the increase in temperature from 220 to 380 K, the effective moment gradually increased to 5.35μ_B. This indicates that the magnetic spin states at 380 K did not fully recover to the HS state of the Fe(III) ions (*ca.* 90% HS, assuming $\mu_{eff}(T)$ = 5.92μ_B).[26] In contrast to solution **1**, complex

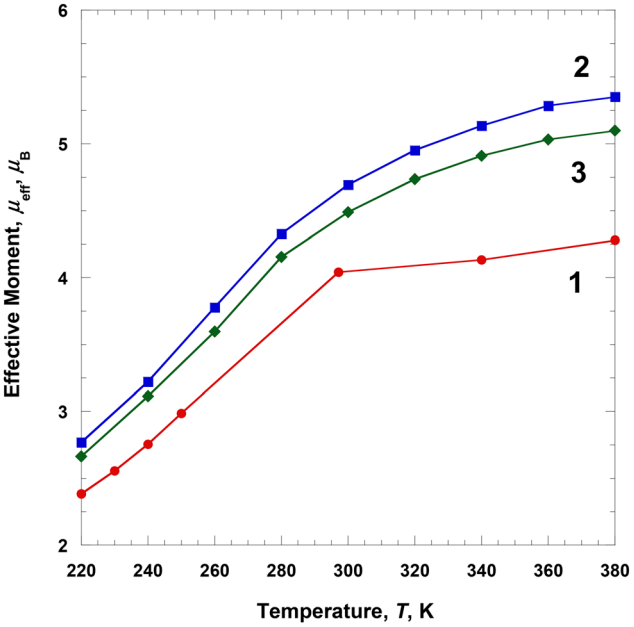

Fig. 6 Temperature dependence of μ_{eff} for **1–3** dissolved in DMF-d_7.

2 showed a clearer SCO as the temperature increased to 380 K, that is, the SCO of solution **2** was different from that of the solid state **2**. At 220 K, the $\mu_{eff}(T)$ value of **3** was *ca.* 2.66μ_B, which is higher than that of the LS Fe(III) ions (S = 1/2) and close to the S = 1 spin state.[25] With an increase in temperature from 220 to 380 K, the effective moment gradually increased to 5.10μ_B. This indicates that the magnetic spin states at 380 K did not fully recover to the HS state of the Fe(III) ions (*ca.* 84% HS, assuming $\mu_{eff}(T)$ = 5.92μ_B).[26] These results are very similar to those of solution **2** and differ from those of solid **3**. In the case of solution **3**, some interactions related to Fe(III) cation, ClO_4^- anion, and DMF solvent significantly affected the SCO behavior.

In solutions **1–3**, all complexes existed as monomeric units without any interactions between their complex cations. We expected that the complex cations would interact with the DMF solvent and their counteranions in solution. Surprisingly, the complexes showed an SCO behavior in solution in the measured temperature range. Although complexes **2** and **3** exhibited an incomplete SCO in the solid state, their SCOs were observed very distinctly in solutions. All complexes exhibited clear SCO behaviors in solution and were expected to relate to weak interactions by the counter ions. The obtained results suggest that the counterions have a more significant effect on SCO than π–π interactions.

Proton relaxation times of 1 and 2

Complexes **1** and **2** were dissolved in DMF-d_7, and the T_1 and T_2 relaxation times of the prepared solutions were measured through NMR at *ca.* 2.90 ppm (Fig. 7). The longitudinal proton relaxation time (T_1) for **1** and **2** was determined at 9.4 T (400 MHz) and 220, 300, 340, and 380 K (Fig. S4 and S6†). The transverse proton relaxation times (T_2) were measured using a

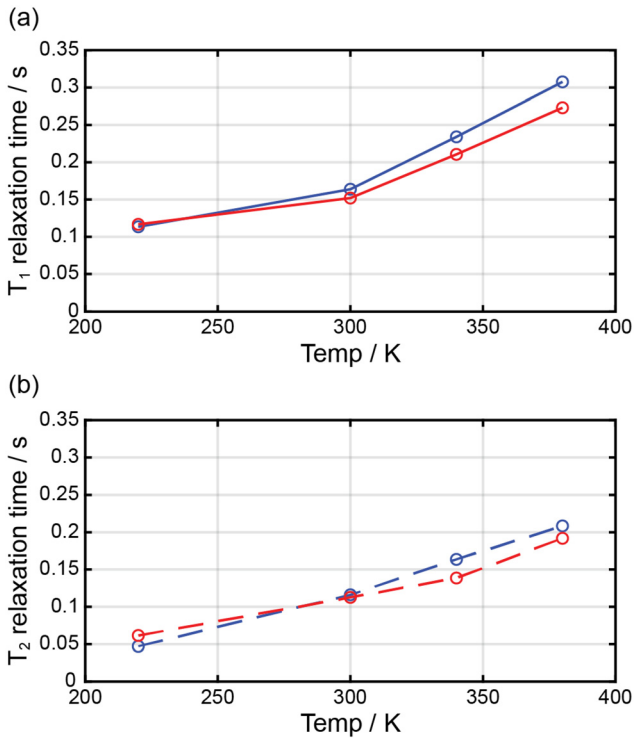

Fig. 7 Temperature dependence of the relaxation times for **1** (blue circle) and **2** (red circle) dissolved in DMF-d_7.

multiecho CPMG pulse sequence (Fig. S5 and S7†). At 220 K, complex **1** showed the T_1 and T_2 relaxation times of 0.11 and 0.047 s, respectively, and the relaxation times gradually increased with a temperature up to 380 K. At 380 K, the T_1 and T_2 relaxation times were 0.31 and 0.21 s, respectively. Thus, from 220 to 380 K, T_1 and T_2 increased by *ca.* 2.8 and 4.5 times, respectively. This means that the ratio of the HS state was proportional to T_1 and T_2. In the case of complex **2**, at 220 K, the T_1 and T_2 relaxation times were 0.12 and 0.061 s, respectively, and an increase in temperature up to 380 K. At 380 K, the T_1 and T_2 relaxation times were 0.27 and 0.19 s, respectively. Thus, from 220 to 380 K, T_1 and T_2 increased by *ca.* 2.3 and 3.1 times, respectively. In **1** and **2**, T_1 was larger than T_2, and both times increased with temperature because of the increase in magnetic moment. T_1 and T_2 depended on the magnetic moments and could potentially be adjusted to MRI contrast agents. The large difference in the T_1/T_2 relaxation times between low and high temperatures can considerably affect contrast in MRI.[28] It is known that weighted MRI images depend on T_1 and T_2. Thus, owing to their temperature-dependent magnetic moments, **1** and **2** may be applied in MRI for diagnostic purposes.[29]

Conclusions

We synthesized a series of mononuclear Fe(III) complexes with two tridentate ligands ($dqmp^-$) and different counteranions; these complexes exhibited SCO behaviors in the solid and solution states. In all three complexes, two $dqmp^-$ ligands were meridionally coordinated in a tridentate manner with one uncoordinated counterion. Their Fe(III) cationic species were isomorphous, although the counterions were different. The solid structures exhibited strong π–π interactions between cationic units. Interestingly, the solid sample with NO_3^- anions showed a very abrupt SCO around 225 K; however, the complexes with BF_4^- and ClO_4^- anions exhibited an incomplete SCO in the solid state. Remarkably, in solutions, Fe(III) complexes with BF_4^- and ClO_4^- anions showed a clearer SCO than that with NO_3^- anions. Furthermore, the T_1 and T_2 relaxation times of the complexes with NO_3^- and BF_4^- depended on the temperature and were proportional to their magnetic moments in solution form. Owing to this behavior, the prepared complexes may potentially be applied as contrast agents in MRI; however, their solubility problems would have to be resolved. In future work, these SCO complexes should be modified and studied to obtain water-soluble species.

Author contributions

Ah Rim Jeong: data curation, investigation, and visualization. Si Ra Park: data curation and investigation. Jong Won Shin: data curation, investigation, and writing – review & editing. Jihyun Kim: data curation and investigation. Ryuya Tokunaga: data curation and investigation. Shinya Hayami: investigation and methodology. Kil Sik Min: funding acquisition, project administration, supervision, and writing – review & editing.

Conflicts of interest

There are no conflicts to declare.

Acknowledgements

This research was supported by the Basic Science Research Program (No. 2021R1F1A1062108) and under the framework of international cooperation program (No. 2021K2A9A2A08000136) through the National Research Foundation of Korea (NRF). X-ray crystallography at the PLS-II 2D-SMC beamline was supported in part by MEST and POSTECH.

References

1 (*a*) Y.-S. Meng and T. Liu, *Acc. Chem. Res.*, 2019, **52**, 1369–1379; (*b*) L. T. Birchall, A. T. Raja, L. Jackson and H. J. Shepherd, *Cryst. Growth Des.*, 2023, **23**, 1768–1774; (*c*) X. Li, D. Zhang, Y. Qian, W. Liu, C. Mathonière, R. Clérac and X. Bao, *J. Am. Chem. Soc.*, 2023, **145**, 9564–9570; (*d*) Y.-C. Sun, F.-L. Chen, K.-J. Wang, Y. Zhao, H.-Y. Wei and X.-Y. Wang, *Inorg. Chem.*, 2023, **62**, 14863–14872; (*e*) T. Kanetomo, K. Yokoyama, Y. Suzuki, H. Ida, A. Okazawa and M. Enomoto, *Dalton Trans.*, 2023, **52**,

12496–12503; (*f*) H.-D. Li, S.-G. Wu and M.-L. Tong, *Chem. Commun.*, 2023, **59**, 6159–6170; (*g*) A. Tsukiashi, K. S. Min, H. Terasawa, S. Yoshinaga, M. Takeda, R. Ohtani, M. Nakamura, L. F. Lindoy and S. Hayami, *Chem. Lett.*, 2018, **47**, 598–600; (*h*) I.-R. Jeon, O. Jeannin, R. Clérac, M. Rouzières and M. Fourmigue, *Chem. Commun.*, 2017, **53**, 4989–4992; (*i*) T. Fujinami, M. Koike, N. Matsumoto, Y. Sunatsuki, A. Okazawa and N. Kojima, *Inorg. Chem.*, 2014, **53**, 2254–2259; (*j*) S. Sundaresan and S. Brooker, *Inorg. Chem.*, 2023, **62**, 12192–12202; (*k*) K. Lee, J. Park, I. Song and S. M. Yoon, *Bull. Korean Chem. Soc.*, 2021, **42**, 1170–1183.

2 (*a*) A. Miyawaki, K. Eda, T. Mochida, T. Sakurai, H. Ohta, T. Nakajima and K. Takahashi, *Inorg. Chem.*, 2021, **60**, 12735–12739; (*b*) Z.-Y. Li, H. Ohtsu, T. Kojima, J.-W. Dai, T. Yoshida, B. K. Breedlove, W.-X. Zhang, H. Iguchi, O. Sato, M. Kawano and M. Yamashita, *Angew. Chem., Int. Ed.*, 2016, **55**, 5184–5189; (*c*) K. Dankhoff and B. Weber, *Dalton Trans.*, 2019, **48**, 15376–15380.

3 (*a*) L. Palagi, E. Di Gregorio, D. Costanzo, R. Stefania, C. Cavallotti, M. Capozza, S. Aime and E. Gianolio, *J. Am. Chem. Soc.*, 2021, **143**, 14178–14188; (*b*) J. Xie, A. Haeckel, R. Hauptmann, I. P. Ray, C. Limberg, N. Kulak, B. Hamm and E. Schellenberger, *Magn. Reson. Med.*, 2021, **85**, 3370–3382; (*c*) M. Lewkowitz, J. Adams, N. S. Sullivan, P. Wang, M. Shatruk, V. Zapf and A. S. Arvij, *Sci. Rep.*, 2023, **13**, 2769.

4 (*a*) M. Nihei, T. Shiga, Y. Maeda and H. Oshio, *Coord. Chem. Rev.*, 2007, **251**, 2606–2621; (*b*) M. A. Halcrow, *Chem. Soc. Rev.*, 2011, **40**, 4119–4142; (*c*) D. J. Harding, P. Harding and W. Phonsri, *Coord. Chem. Rev.*, 2016, **313**, 38–61.

5 D. J. Harding, W. Phonsri, P. Harding, I. A. Gass, K. S. Murray, B. Moubaraki, J. D. Cashion, L. Liu and S. G. Telferd, *Chem. Commun.*, 2013, **49**, 6340–6342.

6 S. A. Sahadevan, E. Cadoni, N. Monni, C. S. de Pipaón, J.-R. G. Mascaros, A. Abhervé, N. Avarvari, L. Marchiò, M. Arca and M. L. Mercuri, *Cryst. Growth Des.*, 2018, **18**, 4187–4199.

7 H.-J. Sheng, C.-C. Xia, X.-Y. Zhang, C.-C. Zhang, W.-J. Ji, Y. Zhao and X.-Y. Wang, *Inorg. Chem.*, 2022, **61**, 12726–12735.

8 B. N. Livesay and M. P. Shores, *Inorg. Chem.*, 2021, **60**, 15445–15455.

9 K. Keisers, H. M. Hüppe, L. Iffland-Mühlhaus, A. Hoffmann, C. Göbel, U.-P. Apfel, B. Weber and S. Herres-Pawlis, *Inorg. Chem.*, 2020, **59**, 15343–15354.

10 S. A. Barrett and M. A. Halcrow, *RSC Adv.*, 2014, **4**, 11240.

11 (*a*) K. Takano, M. Takahashi, T. Fukushima, M. Takezaki, T. Tominaga, H. Akashi, H. Takagi and T. Shibahara, *Bull. Chem. Soc. Jpn.*, 2012, **85**, 1210–1221; (*b*) D. Chakraborty, D. Mandal, V. Ramkumar, V. Subramanian and J. V. Sundar, *Polymer*, 2015, **56**, 157–170.

12 G. A. Bain and G. F. Berry, *J. Chem. Educ.*, 2008, **85**, 532–536.

13 A. J. Arvai and C. Nielsen, *ADSC Quantum-210 ADX Program*, Area Detector System Corporation, Poway, CA, USA, 1983.

14 Z. Otwinowski and W. Minor, in *Methods in Enzymology*, ed. C. W. Carter Jr. and R. M. Sweet, Academic Press, New York, 1997, vol. 276, part A, p. 307.

15 G. M. Sheldrick, *Acta Crystallogr., Sect. A: Found. Crystallogr.*, 1990, **46**, 467–473.

16 G. M. Sheldrick, *Acta Crystallogr., Sect. C: Struct. Chem.*, 2015, **71**, 3–8.

17 A. L. Spek, PLATON program, *Acta Crystallogr., Sect. A: Found. Crystallogr.*, 1990, **46**, 194–201.

18 (*a*) K. De Buysser, G. G. Herman, E. Bruneel, S. Hoste and I. Van Driessche, *Chem. Phys.*, 2005, **315**, 286–292; (*b*) E. M. Schubert, *J. Chem. Educ.*, 1992, **69**, 62; D. F. Evans, *J. Chem. Soc.*, 1959, 2003–2005.

19 K. Nakamoto, *Infrared and Raman Spectra of Inorganic and Coordination Compounds*, John Wiley and Sons, Inc., New Jersey, 6th edn, 2009, part B, pp. 84–120.

20 (*a*) B. J. C. Vieira, J. C. Dias, I. C. Santos, L. C. J. Pereira, V. da Gama and J. C. Waerenborgh, *Inorg. Chem.*, 2015, **54**, 1354–1362; (*b*) R. Díaz-Torres, W. Phonsri, K. S. Murray, L. Liu, M. Ahmed, S. M. Neville, P. Harding and D. J. Harding, *Inorg. Chem.*, 2020, **59**, 13784–13791.

21 (*a*) A. Tsukiashi, M. Nakaya, F. Kobayashi, R. Ohtani, M. Nakamura, J. M. Harrowfield, Y. Kim and S. Hayami, *Inorg. Chem.*, 2018, **57**, 2834–2842; (*b*) J. J. Whittaker, P. Harding, J. K. Clegg and D. J. Harding, *Cryst. Growth Des.*, 2020, **20**, 7006–7011.

22 (*a*) K. Takahashi, T. Sato, H. Mori, H. Tajima and O. Sato, *Phys. B*, 2010, **405**, S65–S68; (*b*) D. J. Harding, D. Sertphon, P. Harding, K. S. Murray, B. Moubaraki, J. D. Cashion and H. Adams, *Chem. – Eur. J.*, 2013, **19**, 1082–1090.

23 N. Ortega-Villar, A. L. Thompson, M. C. Muñoz, V. M. Ugalde-Saldívar, A. E. Goeta, R. Moreno-Esparza and J. A. Real, *Chem. – Eur. J.*, 2005, **11**, 5721–5734.

24 (*a*) P.-C. Yang, K.-P. Yu, C.-T. Hsieh, J. Zou, C.-T. Fang, H.-K. Liu, C.-W. Pao, L. Deng, M.-J. Cheng and C.-Y. Lin, *Chem. Sci.*, 2022, **13**, 9637–9643; (*b*) O. Kahn, *Molecular Magnetism*, VCH, New York, 1993, p. 26.

25 P. B. Tsitovich, F. Gendron, A. Y. Nazarenko, B. N. Livesay, A. P. Lopez, M. P. Shores, J. Autschbach and J. R. Morrow, *Inorg. Chem.*, 2018, **57**, 8364–8374.

26 (*a*) J. W. Shin, A. R. Jeong, S. Jeoung, H. R. Moon, Y. Komatsumaru, S. Hayami, D. Moon and K. S. Min, *Chem. Commun.*, 2018, **54**, 4262–4265; (*b*) K. S. Min, K. Swierczek, A. G. DiPasquale, A. L. Rheingold, W. M. Reiff, A. M. Arif and J. S. Miller, *Chem. Commun.*, 2008, 317–319; (*c*) M. A. Blagov, N. G. Spitsyna, N. S. Ovanesyan, A. S. Lobach, L. V. Zorina, S. V. Simonov, K. V. Zakharov and A. N. Vasiliev, *Dalton Trans.*, 2023, **52**, 1806–1819; (*d*) Z.-J. Ouyang, X.-Y. Mo, J.-Q. Ye, X.-X. Yu, S.-Y. Huang, X.-L. Liu, W.-B. Chen, S. Gao and W. Dong, *Dalton Trans.*, 2021, **50**, 5960–5967.

27 D. Y. Aleshin, I. Nikovskiy, V. V. Novikov, A. V. Polezhaev, E. K. Melnikova and Y. V. Nelyubina, *ACS Omega*, 2021, **6**, 33111–33121.

28 A. Tsukiashi, K. S. Min, H. Kitayama, H. Terasawa, S. Yoshinaga, M. Takeda, L. F. Lindoy and S. Hayami, *Sci. Rep.*, 2018, **8**, 14911.

29 (*a*) M. Yu, B. S. Bouley, D. Xie and E. L. Que, *Dalton Trans.*, 2019, **48**, 9337–9341; (*b*) D. Maheshwaran, T. Nagendraraj, T. S. Balaji, G. Kumaresan, S. S. Kumaran and R. Mayilmurugan, *Dalton Trans.*, 2020, **49**, 14680–14689.